

Geometric Effects on Tunneling in Driven Quantum Systems

Shintaro Takayoshi^{1*}, and Takashi Oka²

¹Department of Physics, Konan University, Kobe 658-8501, Japan

²The Institute for Solid State Physics, The University of Tokyo, Kashiwa, Chiba 277-8581, Japan

We review quantum tunneling provoked by external field driving, focusing on the role of geometric effects. The discussion begins with an overview of tunneling phenomena, including the Landau-Zener model and the Schwinger effect, both of which are essential frameworks to describe the generation of elementary excitation of the system. We also refer to the relation between the modern theory of polarization and the geometry of the system, and introduce the shift vector via adiabatic perturbation theory. Then we introduce the twisted Landau-Zener model and shown how the shift vector modulates tunneling probability, followed by several illustrative applications of this model. We also explain the Keldysh crossover, which is the crossover from a quantum tunneling regime to photon absorption regime in driven systems.

1. Introduction

Tunneling phenomena represent one of the oldest problems in quantum mechanics and have applications in various fields of physics. The Landau-Zener (LZ) model is a prototypical framework that describes transitions in two-level systems near a band anticrossing.^{1–4)} In this model, as the rate of parameter change increases, nonadiabatic transitions become more prominent, and the tunneling probability rises monotonically. Since this problem is related with the manipulation of two-level states, it is important in the fields of spintronics⁵⁾ and quantum computation.^{6,7)} In quantum electrodynamics, a nonperturbative phenomenon of vacuum decay by the application of a strong electric field, which results in the spontaneous creation of particle-antiparticle pairs, has been proposed by Heisenberg and Euler⁸⁾ and later refined by Schwinger.⁹⁾ This phenomenon can be understood from the viewpoint of quantum tunneling in the Dirac model with the integration over the momentum space. This effect is important for understanding the interplay between quantum fluctuations and electromagnetic field and its implications are applied to many significant quantum phenomena in high-energy physics, astrophysics, and condensed matter physics, such as dielectric breakdown in semiconductors^{4,10)} and Mott insulators,^{11–16)} and the Kibble-Zurek mechanism.^{17–19)} The Schwinger effect can be extended to the AC fields,^{20–22)} which is related with the problems of strong field ionization^{23–26)} and a particle escaping from an oscillating trap.²⁷⁾

Another topic gathering attention in recent years is the effect of geometry on physical properties. Geometric phases such as the Berry phase^{28,29)} play a crucial role in phenomena like the quantum Hall effect^{30,31)} and topological insulators.^{32,33)} Their influence on nonlinear electronic processes has also attracted interest, including the nonlinear Hall effect³⁴⁾ and the emergence of even-order nonlinear optical responses and shift currents in crystals with broken inversion symmetry.^{35,36)} In addition, Floquet engineering³⁷⁾ provides a powerful framework for realizing topological states in nonequilibrium systems.^{38–40)}

The influence of geometric effects in dynamics goes be-

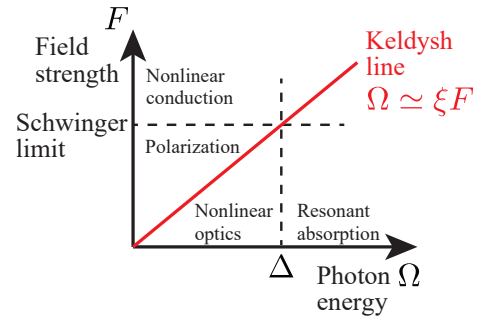


Fig. 1. Various phenomena provoked by the application of external AC fields in the parameter space of photon energy Ω and field strength F . ξ and Δ are the correlation length and the gap of the system, respectively. The change of behavior over the Keldysh line $\Omega \approx \xi F$ is called the Keldysh crossover.

yond the contribution to the phase factor.^{28,41)} It is pointed out that the geometry affects the tunneling probability in nonadiabatic transition processes through the geometric amplitude factor.^{42–44)} This effect has been applied to the counterdiabatic driving of the system.^{45–47)}

When considering excitations of a system driven by an external field, two types of mechanisms come into play: quantum tunneling and photon absorption. The dominant mechanism is determined by the field strength F and the angular frequency Ω of the driving field [Fig. 1]. The quantum tunneling regime and the photon absorption regime are separated by the Keldysh line $\Omega \approx \xi F$, where ξ represents the correlation length of the system. By varying these parameters, the transition between the two regimes, known as the Keldysh crossover, is observed.²⁷⁾

This paper aims to review quantum tunneling induced by external field driving and the role of geometry in nonadiabatic excitation, especially the geometric amplitude factor. To this end, we introduce a twisted LZ (TLZ) model, discuss its properties, and demonstrate several examples of its applications. We also address the Keldysh crossover in many-body systems.

*takayoshi@konan-u.ac.jp

This paper is organized as follows. In Sec. 2, we review tunneling phenomena, particularly focusing on the LZ model and the Schwinger effect. We also discuss the modern theory of polarization, which is related to geometry, and introduce the concept of the shift vector by reviewing adiabatic perturbation theory. In Sec. 3, we introduce the TLZ model and demonstrate how the shift vector influences the tunneling probability. Several applications of the TLZ model are presented in Sec. 4. Section 5 provides an explanation of the Keldysh crossover. Finally, a summary and discussion is presented in Sec. 6.

2. Excitation by tunneling phenomena and geometric effects

2.1 Quantum tunneling

First, we explain about the excitations generated by quantum tunneling. One of the simplest models to describe the tunneling phenomena is the LZ model:^{1,3,4)}

$$\hat{H}_{\text{LZ}}(t) = m\hat{\sigma}^z + vq(t)\hat{\sigma}^x, \quad q(t) = -Ft, \quad (1)$$

where m and v are constant, $\hat{\sigma}^j$ is the Pauli matrices, and $q(t)$ is swept linearly in the time interval $-\infty < t < \infty$. In this paper, we employ the unit $c = \hbar = 1$. The profile of the instantaneous Hamiltonian is a two-level system with avoided crossing, and the gap is $\sqrt{m^2 + (vq(t))^2}$ taking the minimum at $t = 0$. During this process, the lower energy initial state makes a tunneling transition to the higher energy one, and its probability is obtained analytically as

$$P(F) = \exp\left[-\pi \frac{m^2}{|vF|}\right]. \quad (2)$$

In the limit of $|F| \rightarrow 0$, $P(F)$ approaches zero, which is the adiabatic limit.

In the quantum electrodynamics, an analogous phenomenon happens in the creation process of electron-positron pairs from the vacuum in the strong DC electric field \mathbf{F} , so-called the Schwinger effect. It can be formulated as a massive Dirac model

$$\hat{\mathcal{H}}_{\text{D}} = v \sum_{j=x,y,z} \hat{\gamma}^0 \hat{\gamma}^j (k_j + e_0 A_j) + m \hat{\gamma}^0, \quad (3)$$

where $-e_0$ is the charge of electron, $\mathbf{A} = -\mathbf{F}t$ is the vector potential, and $\hat{\gamma}^\mu$ ($\mu = 0, x, y, z$) are the gamma matrices $\hat{\gamma}^0 = \begin{pmatrix} 0 & I \\ I & 0 \end{pmatrix}$, $\hat{\gamma}^j = \begin{pmatrix} 0 & \hat{\sigma}^j \\ -\hat{\sigma}^j & 0 \end{pmatrix}$ ($j = x, y, z$). For each wave number \mathbf{k} , the generation of an electron-positron pair is regarded as a tunneling process from the lower to upper band. Schwinger estimated the total pair production rate at the one-loop order as⁹⁾

$$\Gamma \propto \sum_{n=1}^{\infty} \frac{1}{n^2} \exp\left(-\frac{\pi m^2 n}{ve_0 |\mathbf{F}|}\right). \quad (4)$$

Thus electron-positron pairs proliferate when the electric field strength is above the threshold

$$F_{\text{th}} = m^2/(ve_0), \quad (5)$$

which is called the Schwinger limit.^{8,9,48)}

2.2 Schwinger effects and polarization from the geometric viewpoint

Next we explain the modern formulation of polarization and discuss its relation with the Schwinger effect. King-Smith and Vanderbilt proposed an expression of polarization in terms of a geometric property of states:^{49,50)}

$$\mathbf{P}_e = -\frac{e_0}{(2\pi)^3} \sum_{n:\text{occ}} \int_{\text{BZ}} i \langle u_{n,\mathbf{k}} | \nabla_{\mathbf{k}} | u_{n,\mathbf{k}} \rangle d\mathbf{k}, \quad (6)$$

where $i \langle u_{n,\mathbf{k}} | \nabla_{\mathbf{k}} | u_{n,\mathbf{k}} \rangle$ represents the Berry connection, $u_{n,\mathbf{k}}$ is the periodic part of the wave function, and the summation is taken over the occupied bands. In the following, we focus on the 1D case for simplicity, where $P_e = -\frac{e_0}{2\pi} \sum_{n:\text{occ}} \int_{\text{BZ}} i \langle u_{n,k} | \partial_k | u_{n,k} \rangle dk$. This expression avoids ambiguities in crystals under the periodic boundary condition in contrast to the traditional way of calculation based on charge distributions. Resta extended this approach to general quantum states^{51,52)} using the twist operator:

$$P_e = \frac{e_0}{2\pi} \text{Im} \ln \langle \Psi_0 | e^{i\frac{2\pi}{L}\hat{X}} | \Psi_0 \rangle, \quad (7)$$

where $\hat{X} = \sum_r r \hat{n}_r$ is the position operator (\hat{n}_r is the number operator) and L is the system size. The twist operator $e^{i\frac{2\pi}{L}\hat{X}}$ shifts the state in the momentum space, and it is used for discussing the Lieb-Schultz-Mattis theorem.^{53–56)} The polarization of one-dimensional (1D) insulators acts as a topological index under the symmetry constraint of the system.^{57,58)} For example, if the system has inversion symmetry, the polarization value takes discrete values of 0 or 1/2, which indicate whether the system is in a trivial or topological phase.

Now we discuss the relation between Schwinger effects and polarization in terms of the geometry.^{12,59)} The Hamiltonian of a system in a DC electric field in the potential gauge is given as $\hat{\mathcal{H}} = \hat{\mathcal{H}}_0 + e_0 F \hat{X}$. We consider the time evolution by the Hamiltonian $\hat{\mathcal{H}}$ with the initial state $|\Psi_0\rangle$, which is the ground state of $\hat{\mathcal{H}}_0$. Then the state is given by $|\Psi(t)\rangle = e^{-it(\hat{\mathcal{H}}_0 + e_0 F \hat{X})} |\Psi_0\rangle$. The transition amplitude from $|\Psi_0\rangle$ to $e^{-i\hat{\mathcal{H}}_0 t} |\Psi_0\rangle$ through this time evolution is represented as

$$\begin{aligned} \Xi(t) &= \langle \Psi_0 | e^{i\hat{\mathcal{H}}_0 t} |\Psi(t)\rangle \\ &= \langle \Psi_0 | e^{-it(\hat{\mathcal{H}}_0 + e_0 F \hat{X})} |\Psi_0\rangle e^{itE_0}, \end{aligned} \quad (8)$$

where E_0 is the ground state energy of $\hat{\mathcal{H}}_0$. The effective Lagrangian can be asymptotically defined as

$$\Xi(t) \sim e^{itL\mathcal{L}(F)}. \quad (9)$$

In Eq. (8),

$$\langle \Psi_0 | e^{-it(\hat{\mathcal{H}}_0 + e_0 F \hat{X})} |\Psi_0\rangle = \langle \Psi_0 | e^{-i\hat{\mathcal{H}}_0 t} e^{-ite_0 F \hat{X}} e^{O(F^2)} |\Psi_0\rangle, \quad (10)$$

from the Baker-Campbell-Hausdorff formula since $\hat{\mathcal{H}}_0$ is just a c-number E_0 for the commutation relation containing only one $e_0 F \hat{X}$ term inside the expectation value $\langle \Psi_0 | \cdot | \Psi_0 \rangle$. Here we set $t = 2\pi/(Le_0 F)$ and take the limit of $F \rightarrow 0$, then $\lim_{F \rightarrow 0} \Xi(2\pi/(Le_0 F)) = \langle \Psi_0 | e^{-i\frac{2\pi}{L}\hat{X}} | \Psi_0 \rangle = (\langle \Psi_0 | e^{i\frac{2\pi}{L}\hat{X}} | \Psi_0 \rangle)^*$. Hence, the transition probability is related with the polarization Eq. (7) as

$$P_e = -\lim_{F \rightarrow 0} \frac{e_0}{2\pi} \text{Im} \ln \Xi\left(\frac{2\pi}{Le_0 F}\right). \quad (11)$$

By using the effective Lagrangian Eq. (9), this expression is

recast into

$$P_c = -\lim_{F \rightarrow 0} \frac{1}{F} \text{Re} \mathcal{L}(F) = -\left. \frac{\partial \text{Re} \mathcal{L}(F)}{\partial F} \right|_{F=0}. \quad (12)$$

2.3 Geometric effects in the adiabatic perturbation theory

In this subsection, we describe the Geometric effects from the viewpoint of the adiabatic perturbation theory. We consider the time dependent-Hamiltonian of two-level systems

$$\hat{\mathcal{H}}(t) = \mathbf{d}(q(t)) \cdot \hat{\boldsymbol{\sigma}}, \quad (13)$$

where $q(t) = k + e_0 F t$. It is assumed that the gap does not close for the whole time interval. The instantaneous eigenenergy $E_{\pm}(t)$ ($E_+(t) > E_-(t)$) and eigenstates $|u_{\pm}(t)\rangle$ are defined as

$$\hat{\mathcal{H}}(t) |u_{\pm}(t)\rangle = E_{\pm}(t) |u_{\pm}(t)\rangle. \quad (14)$$

We expand the solution of the Schrödinger equation in the basis of $|u_{\pm}(t)\rangle$ as

$$|\psi(t)\rangle = \sum_{n=\pm} a_n(t) e^{-i \int_0^t ds \{E_n(s) - e_0 F A_{nn}(s)\}} |u_n(t)\rangle, \quad (15)$$

where

$$A_{nm}(t) = \langle u_n(t) | i \partial_t | u_m(t) \rangle = \frac{1}{e_0 F} \langle u_n(t) | i \partial_t | u_m(t) \rangle \quad (16)$$

stands for the Berry connection. Substituting Eq. (15) into the Schrödinger equation

$$i \partial_t |\psi(t)\rangle = \hat{\mathcal{H}}(t) |\psi(t)\rangle, \quad (17)$$

we obtain

$$\begin{aligned} & \sum_{n=\pm} (i \partial_t a_n(t)) e^{-i \int_0^t ds \{E_n(s) - e_0 F A_{nn}(s)\}} |u_n(t)\rangle \\ & - \sum_{n=\pm} a_n(t) e^{-i \int_0^t ds \{E_n(s) - e_0 F A_{nn}(s)\}} e_0 F A_{nn}(t) |u_n(t)\rangle \\ & + \sum_{n=\pm} a_n(t) e^{-i \int_0^t ds \{E_n(s) - e_0 F A_{nn}(s)\}} (i \partial_t |u_n(t)\rangle) = 0. \end{aligned} \quad (18)$$

By applying $\langle u_+(t) |$ and $\langle u_-(t) |$ to Eq. (18), we derive the equations

$$\begin{aligned} i \partial_t a_+(t) &= -a_-(t) e_0 F A_{+-}(t) \\ & \times e^{i \int_0^t ds \{E_+(s) - E_-(s) - e_0 F A_{++}(s) + e_0 F A_{--}(s)\}}, \end{aligned} \quad (19)$$

$$\begin{aligned} i \partial_t a_-(t) &= -a_+(t) e_0 F A_{-+}(t) \\ & \times e^{-i \int_0^t ds \{E_+(s) - E_-(s) - e_0 F A_{++}(s) + e_0 F A_{--}(s)\}}. \end{aligned} \quad (20)$$

Here we introduce a gauge independent quantity called geometric amplitude factor

$$R_{nm}(t) = -A_{nn}(t) + A_{mm}(t) + \partial_q \arg A_{nm}(t), \quad (21)$$

which is introduced by Berry.⁴²⁾ Then the equations become

$$\begin{aligned} i \partial_t a_+(t) &= -a_-(t) e_0 F |A_{+-}(t)| \\ & \times e^{i \int_0^t ds \{E_+(s) - E_-(s) + e_0 F R_{+-}(s) + i \arg A_{+-}(0)\}}, \end{aligned} \quad (22)$$

$$\begin{aligned} i \partial_t a_-(t) &= -a_+(t) e_0 F |A_{-+}(t)| \\ & \times e^{-i \int_0^t ds \{E_+(s) - E_-(s) - e_0 F R_{+-}(s) + i \arg A_{+-}(0)\}}. \end{aligned} \quad (23)$$

Here we have used $e^{-i \arg A_{+-}(t)} A_{+-}(t) = |A_{+-}(t)|$ and $e^{-i \arg A_{-+}(t)} A_{-+}(t) = |A_{-+}(t)|$. With the initial condition $a_-(0) =$

1 and $a_+(0) = 0$, the solution is written in the integral form as

$$\begin{aligned} a_+(t) &= i \int_0^t ds a_-(s) e_0 F |A_{+-}(s)| \\ & \times e^{i \int_0^s ds' \{E_+(s') - E_-(s') + e_0 F R_{+-}(s') + i \arg A_{+-}(0)\}}, \end{aligned} \quad (24)$$

$$\begin{aligned} a_-(t) &= i \int_0^t ds a_+(s) e_0 F |A_{-+}(s)| \\ & \times e^{-i \int_0^s ds' \{E_+(s') - E_-(s') - e_0 F R_{+-}(s') + i \arg A_{+-}(0)\}}. \end{aligned} \quad (25)$$

The formal solution is given by substituting a_{\pm} in the right hand sides iteratively. Using the first order iterative approximation, i.e., $a_-(t) \simeq 1$,

$$\begin{aligned} a_+(t) &= i e^{i \arg A_{+-}(0)} \int_0^t ds e_0 F |A_{+-}(s)| \\ & \times e^{i \int_0^s ds' \{E_+(s') - E_-(s') + e_0 F R_{+-}(s')\}}. \end{aligned} \quad (26)$$

The integration in Eq. (26) can be evaluated by the Dykhne-Davis-Pechukas (DDP) method^{60–62)} also known as the Landau-Dykhne method. In the DDP method, the integration is performed in the space of wave number extended to the complex plane. In this complex wave number space, an exceptional point k_c , where the excitation gap is closed, can be reached by proceeding in the imaginary direction from the gap minimum point on the real axis k_0 . Recently the extension of the DDP formula is discussed in terms of the Lefschetz-thimble analysis.⁶³⁾ After evaluating the integration in Eq. (26) by the DDP method, the tunneling probability is calculated to be

$$\begin{aligned} P(F) &= |a_+(t)|^2 \\ &\simeq \exp \left[2 \text{Im} \int_{k_0}^{k_c} dk \frac{E_+ - E_- + e_0 F R_{+-}}{e_0 |F|} \right]. \end{aligned} \quad (27)$$

This formula indicates that the tunneling probability is modulated by the geometric amplitude factor as pointed out by Berry.⁴²⁾ The expression of $E_+ - E_-$, $|A_{+-}|$, and R_{+-} in Eq. (13) for the parameter curve $\mathbf{d}(q(t))$ is provided in Ref.⁶⁴⁾ We give the extension of Eq. (27) which includes the $O(R_{+-}^2)$ term in Sec. 3.

Geometric amplitude factor Eq. (21) is also called quantum geometric potential.^{65,66)} In the expression of polarization in terms of the Berry phase, $R_{nm}(q)$, which is Eq. (21) represented as a function of the crystal momentum q , is known as the shift vector. The shift vector R_{+-} quantifies the difference of the electric polarization between the upper and lower bands.³⁵⁾ In Ref.,⁶⁴⁾ Eq. (27) is applied to the Rice-Mele model to discuss the nonreciprocal tunneling. The multiple tunneling effect in nonreciprocal LZ tunneling has been studied recently.⁶⁷⁾

3. Twisted LZ model

To demonstrate the nonadiabatic geometric effects, we introduce a simple time-dependent Hamiltonian of a two-level system,

$$\hat{\mathcal{H}}(q(t)) = m \hat{\sigma}^z + v q(t) \hat{\sigma}^x + \frac{1}{2} \kappa_{\parallel} v^2 q(t)^2 \hat{\sigma}^y, \quad q(t) = -F t \quad (28)$$

where m and v are constant. Since the $q(t)^2$ term is added to the LZ model Eq. (1), we call Eq. (28) the twisted LZ (TLZ) model.

In the notation of Eq. (13),

$$\mathbf{d}(q(t)) = (vq(t), \frac{1}{2}\kappa_{\parallel}v^2q(t)^2, m) \quad (29)$$

draws a parabolic trajectory in the three-dimensional (3D) space while the standard LZ model ($\kappa_{\parallel} = 0$) draws a straight line. Note that κ_{\parallel} is the curvature of the parabola at the vertex, where the gap of the system takes the minimum.

3.1 Tunneling probability

We analyze the tunneling probability of Eq. (28), by utilizing the time-dependent unitary transformation, which corresponds to changing the frame of the system. Let us consider the unitary transformation $|\psi(t)\rangle = \hat{U}(t)|\psi'(t)\rangle$. Substituting this relation into the Schrödinger equation Eq. (17), we obtain $i\partial_t \hat{U}(t)|\psi'(t)\rangle + \hat{U}(t)i\partial_t |\psi'(t)\rangle = \hat{\mathcal{H}}(t)\hat{U}(t)|\psi'(t)\rangle$, which is finally rewritten as

$$i\partial_t |\psi'(t)\rangle = [\hat{U}^\dagger(t)\hat{\mathcal{H}}(t)\hat{U}(t) - \hat{U}^\dagger(t)(i\partial_t \hat{U}(t))]| \psi'(t)\rangle. \quad (30)$$

Hence the effective Hamiltonian in the $|\psi'(t)\rangle$ frame is

$$\hat{\mathcal{H}}_{\text{eff}}(t) = \hat{U}^\dagger(t)\hat{\mathcal{H}}(t)\hat{U}(t) - \hat{U}^\dagger(t)(i\partial_t \hat{U}(t)). \quad (31)$$

This time-dependent unitary transformation is useful for analyzing the dynamics of quantum systems in terms of an effective static model.^{68,69)}

In the present case, we transform the TLZ model into the standard LZ model using a time-dependent rotation about the d_z axis $\hat{U}(t) = e^{i\frac{\theta(q(t))}{2}\hat{\sigma}^z}$, where

$$\theta(q(t)) = -\arctan \frac{d_y(q(t))}{d_x(q(t))} = -\arctan \frac{1}{2}\kappa_{\parallel}vq(t) \quad (32)$$

is the rotation angle [Fig. 2(a)]. Since the tunneling happens mainly around the gap minimum point $q = 0$, we expand

$$\theta(q) \simeq -\frac{1}{2}\kappa_{\parallel}vq + O(q^3). \quad (33)$$

Substituting Eq. (32) into Eq. (31), we derive an effective Hamiltonian

$$\hat{\mathcal{H}}_{\text{eff}}(t) = \left(m + \frac{\kappa_{\parallel}vF}{4}\right)\hat{\sigma}^z + (vq + O(q^3))\hat{\sigma}^x, \quad (34)$$

where the $\hat{U}^\dagger(t)(i\partial_t \hat{U}(t))$ term gives $-\frac{1}{2}\frac{dq}{dt}\frac{d\theta(q)}{dq}\hat{\sigma}^z = (-\frac{\kappa_{\parallel}vF}{4} + O(q^3))\hat{\sigma}^z$. Therefore, for a linear sweep $q = -Ft$, the tunneling probability $P(F)$ in Eq. (28) becomes

$$P(F) = \exp\left[-\pi \frac{(m + \kappa_{\parallel}vF/4)^2}{|vF|}\right]. \quad (35)$$

For the model Eq. (28), the geometric amplitude factor Eq. (21) is calculated to be $R_{+-}(t=0) = \kappa_{\parallel}v$. Hence, Eq. (35) is rewritten as

$$P(F) = \exp\left[-\pi \frac{(m + R_{+-}F/4)^2}{|vF|}\right]. \quad (36)$$

In Eq. (36), we notice that the tunneling gap is effectively modified by the geometric amplitude factor as $\Delta_{\text{eff}} = 2m + \kappa_{\parallel}vF/2$. This result is the improvement of Eq. (27) with $e_0 = 1$ by including the $O(R_{+-}^2)$ term in the exponential.

Here, we have considered the case that the positional vector of the gap minimum in the parameter space $(0, 0, m)$ is

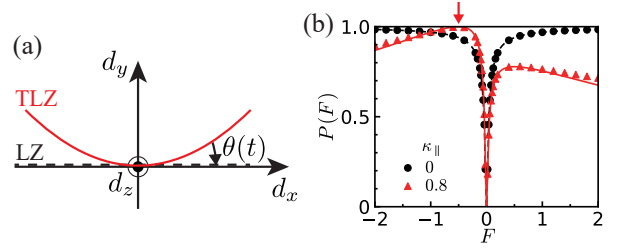


Fig. 2. (a) Time-dependent rotation which transforms the TLZ model into the LZ model. (b) Tunneling probability of the model Eq. (28) with $m = 0.1$ and $v = 1$. Numerically calculated $P(F)$ is shown by circles (the LZ model $\kappa_{\parallel} = 0$) and triangles (the TLZ model $\kappa_{\parallel} = 0.8$). The dashed and solid lines are the predictions from Eq. (35) for the LZ and TLZ models, respectively. The arrow represents the sweeping speed at which the perfect tunneling happens Eq. (40).

perpendicular to the plane which contains the neighborhood of the curve $\mathbf{d}(q)$ around the gap minimum. We can extend the above discussion to the general parameter curve

$$\hat{\mathcal{H}}(t) = \hat{A} + \hat{B}q(t) + \hat{C}q(t)^2/2, \quad (37)$$

where the conditions $\{\hat{A}, \hat{B}\} = 0$ and $\{\hat{B}, \hat{C}\} = 0$ are required in order for the energy gap and the absolute value of velocity to be minimal at $q(t) = 0$. We can apply Eq. (35) to the curve Eq. (37) by using the parameters⁷⁰⁾

$$m = \|\hat{A}\|, \quad v = \|\hat{B}\|, \quad \kappa_{\parallel}v^2 = -\frac{i}{8} \frac{\text{Tr}\{\hat{A}, \hat{B}, \hat{C}\}}{\|\hat{A}\|\|\hat{B}\|}, \quad (38)$$

where $\|\hat{O}\| \equiv \frac{1}{2}\sqrt{\text{Tr}\{\hat{O}, \hat{O}\}}$.

3.2 Numerical demonstration

We numerically calculate the time evolution of the TLZ model Eq. (28) and evaluate the tunneling probability for various sweeping speed. In Fig. 2(b), the circles and triangles show the numerically calculated results, and the dashed and solid lines show the predictions from Eq. (35). Comparing the circles and dashed line (the LZ model $\kappa_{\parallel} = 0$) with the triangles and solid line (the TLZ model $\kappa_{\parallel} = 0.8$), we notice several anomalous phenomena in the TLZ model.

The first is the rectification or nonreciprocity, i.e., the tunneling probability depends on the direction of the sweep. From Eq. (35), the ratio of tunneling probabilities between two sweep directions is evaluated as

$$P(|F|)/P(-|F|) = \exp(-\pi m \kappa_{\parallel}). \quad (39)$$

This phenomenon arises from the $O(\kappa_{\parallel})$ term in the exponential and has been indicated by Berry.⁴²⁾

The second is that the perfect tunneling $P = 1$ takes place as shown by an arrow in Fig. 2(b). As we can see from Eq. (35), it happens when the sweeping speed is

$$F_{\text{PT}} = -\frac{4m}{\kappa_{\parallel}v}, \quad (40)$$

where the modified gap $(2m + \kappa_{\parallel}vF/2)$ becomes zero and the system effectively shows a gapless behavior.

The third is the counterdiabaticity. In Fig. 2(b), $P(F)$ decreases as $|F|$ increases in the large $|F|$ region for the TLZ case while $P(F)$ increases monotonically as $|F|$ increases for

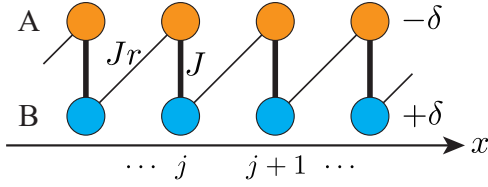


Fig. 3. The schematic picture of the saw-tooth chain model Eq. (42).

the standard LZ case. From Eq. (35), the tunneling probability behaves as $P(F) \simeq \exp(-\pi\kappa_{\parallel}^2|vF|/16)$ in the large $|F|$ regime.

4. Application of twisted LZ model

4.1 Single spin in time-dependent external magnetic field

The simplest application of the TLZ model is the isolated spin-1/2 in the magnetic field $\mathbf{h}(t)$. The external field is static in the z direction and time-dependent on the xy plane: $\mathbf{h}(t) = (\alpha t, \beta t^2, h_z)$. The Hamiltonian is given as

$$\hat{\mathcal{H}}(t) = -\alpha t \hat{S}^x - \beta t^2 \hat{S}^y - h_z \hat{S}^z, \quad (41)$$

which is the same as the TLZ model Eq. (28). For simplicity, we assume $\alpha > 0$, $\beta > 0$, and $h_z > 0$. At the initial $t \rightarrow -\infty$ and final $t \rightarrow \infty$ time, the lower (higher) energy state corresponds to the spin in the $+y$ ($-y$) direction. Thus, through the TLZ process, the tunneling from the lower to higher energy state is the spin-flip. Finding an optimal modulation of external field is an important task for the high-speed spin control. From such viewpoint, counterdiabatic driving of quantum states have been studied.^{71,72)} The magnetization process in quantum spin systems is also regarded as tunneling.^{73,74)}

Recently, spin control by the TLZ process is realized in nitrogen-vacancy centers of diamond.⁷⁵⁾ When an electron is captured at a point defect consisting of a nitrogen atom and a vacancy in diamond, the spin triplet states $m_S = 1, 0, -1$ are formed. They use $m_S = 0$ and -1 states as a two-level system and realize the TLZ model Eq. (41) by applying an appropriate microwave pulse. The tunneling probability is measured by changing the sweep velocity and the results show the behavior of the TLZ model including the nonreciprocity and the perfect tunneling.

4.2 Saw-tooth chain model

Next we consider a simple 1D lattice model which can be understood in terms of twisted LZ mechanism. As shown in Fig. 3, the lattice is a two-leg ladder with the rung index j and the chain index $\{A, B\}$. The hopping only exists between the sites (j, A) and (j, B) , and between (j, B) and $(j+1, A)$ like a shape of the saw-tooth, thus we call this model as the saw-tooth chain model. The Hamiltonian is represented as

$$\begin{aligned} \hat{\mathcal{H}} = \sum_j [& -J(\hat{a}_{j,A}^\dagger \hat{a}_{j,B} + \text{H.c.}) - Jr(\hat{a}_{j,B}^\dagger \hat{a}_{j+1,A} + \text{H.c.}) \\ & - \delta \hat{a}_{j,A}^\dagger \hat{a}_{j,A} + \delta \hat{a}_{j,B}^\dagger \hat{a}_{j,B}]. \end{aligned} \quad (42)$$

After the Fourier transformation

$$\hat{a}_k = \sqrt{\frac{1}{N}} \sum_j e^{ikj} \hat{a}_{j,A}, \quad \hat{b}_k = \sqrt{\frac{1}{N}} \sum_j e^{ikj} \hat{a}_{j,B}, \quad (43)$$

the Hamiltonian is written in the form of

$$\mathcal{H} = \sum_k \begin{pmatrix} \hat{a}_k^\dagger & \hat{b}_k^\dagger \end{pmatrix} \hat{\mathcal{H}}(k) \begin{pmatrix} \hat{a}_k \\ \hat{b}_k \end{pmatrix}, \quad (44)$$

where

$$\begin{aligned} \hat{\mathcal{H}}(k) &= \begin{pmatrix} -\delta & -J(1 + re^{ik}) \\ -J(1 + re^{-ik}) & \delta \end{pmatrix} \\ &= -J(1 + r \cos k) \hat{\sigma}^x + (Jr \sin k) \hat{\sigma}^y - \delta \hat{\sigma}^z. \end{aligned} \quad (45)$$

When the uniform static electric field F is applied to this system, the Hamiltonian becomes $\hat{\mathcal{H}}(k + A) = \hat{\mathcal{H}}(k - Ft)$ (we set $e_0 = 1$) We expand Eq. (45) around the gap minimum $k = \pi$ up to the second order

$$\mathcal{H}(k') = -J(1 - r) \hat{\sigma}^x - \delta \hat{\sigma}^z - Jr \hat{\sigma}^y k' - \frac{Jr}{2} \hat{\sigma}^x k'^2, \quad (46)$$

where $k' = k - \pi$. Thus the TLZ model is realized for each crystal wavenumber k and we can evaluate the tunneling probability $\mathcal{P}(F, k)$. In the actual model, the gap minimum is located periodically $k = \pi(2n + 1)$ (n : integer) and the interband interference happens. Furthermore, the population of electrons in the upper and lower bands is determined from the relaxation process. Here, for simplicity, we assume that the population of electrons in the upper band is proportional to $\mathcal{P}(F, k)$, which corresponds to the application of the relaxation time approximation. The improvement of the relaxation time approximation in the LZ tunneling has been proposed recently.^{76,77)} Since the physical quantities are calculated through the integration over the crystal wave number k , we can observe the “twisted Schwinger effect” in this system. For example, electric current is proportional to

$$J_c(F) \propto \int dk k \mathcal{P}(F, k). \quad (47)$$

We substitute

$$\begin{aligned} m &= \sqrt{J^2(1 - r)^2 + \delta^2}, \quad v = Jr \\ \kappa_{\parallel} v^2 &= \frac{Jr\delta}{\sqrt{J^2(1 - r)^2 + \delta^2}} \end{aligned} \quad (48)$$

which is obtained from Eq. (38), into Eq. (35). The tunneling probability becomes

$$\begin{aligned} \mathcal{P}(F, k) &= \exp \left[-\frac{\pi}{Jr|F|} \left\{ \sqrt{J^2(1 - r)^2 + \delta^2} \right. \right. \\ &\quad \left. \left. - \frac{F\delta}{4\sqrt{J^2(1 - r)^2 + \delta^2}} \right\}^2 \right], \end{aligned} \quad (49)$$

which does not depend on k . Therefore the rectification is predicted to happen in this system as

$$\frac{J_c(|F|)}{J_c(-|F|)} = \exp\left(\frac{\pi\delta}{Jr}\right). \quad (50)$$

The saw-tooth model looks a little artificial, but its properties are quite similar to the Rice-Mele model⁷⁸⁾

$$\begin{aligned} \hat{\mathcal{H}}_{\text{RM}} &= \sum_j [(-t + \gamma)(\hat{a}_{2j}^\dagger \hat{a}_{2j+1} + \hat{a}_{2j+1}^\dagger \hat{a}_{2j}) \\ &\quad + (-t - \gamma)(\hat{a}_{2j+1}^\dagger \hat{a}_{2j+2} + \hat{a}_{2j+2}^\dagger \hat{a}_{2j+1}) \\ &\quad - \delta \hat{a}_{2j}^\dagger \hat{a}_{2j} + \delta \hat{a}_{2j+1}^\dagger \hat{a}_{2j+1}], \end{aligned} \quad (51)$$

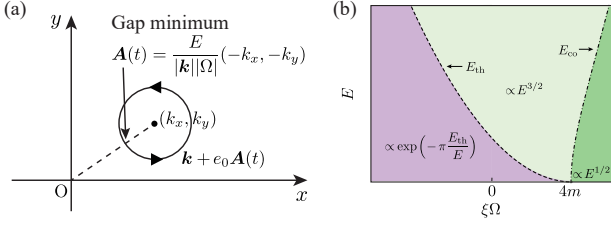


Fig. 4. (a) The gap minimum point in the wave number space. (b) The behavior of the total pair production rate Γ_ξ in the parameter space of $\xi\Omega$ and E .

which is a well-known model for topological insulators.^{79,80} The distinction between the saw-tooth and Rice-Mele models is that, in the former, a pair of sites share the same position along the x axis, whereas in the latter, each site occupies a different position. The Rice-Mele model was analyzed by a nonreciprocal LZ model in Ref.⁶⁴

We also note that the 1D lattice electron model can be mapped to the corresponding $S = 1/2$ spin chain model through the Jordan-Wigner transformation:

$$\begin{aligned} \hat{S}_l^z &= \hat{n}_l - \frac{1}{2}, \\ \hat{S}_l^+ &= \hat{a}_l^\dagger \prod_{j=1}^{l-1} (1 - 2\hat{n}_j), \quad \hat{S}_l^- = \hat{a}_l \prod_{j=1}^{l-1} (1 - 2\hat{n}_j), \end{aligned} \quad (52)$$

where $\hat{n}_j \equiv \hat{a}_j^\dagger \hat{a}_j$. Using this transformation, we can map the saw tooth model Eq. (42) into a spin chain model with bond alternation and staggered field:

$$\begin{aligned} \hat{H} = \sum_j [& -J(\hat{S}_{j,A}^x \hat{S}_{j,B}^x + \hat{S}_{j,A}^y \hat{S}_{j,B}^y) \\ & - J_r(\hat{S}_{j,B}^x \hat{S}_{j+1,A}^x + \hat{S}_{j,B}^y \hat{S}_{j+1,A}^y) \\ & - \delta \hat{S}_{j,A}^z + \delta \hat{S}_{j,B}^z]. \end{aligned} \quad (53)$$

In this mapping, the electric field corresponds to magnetic field gradient along the S^z axis, and electric current corresponds to spin current. Multiferroic materials have been studied by the effective spin models, and the generation of electric shift current by electromagnons⁸¹ and spin shift current⁸² have been proposed theoretically. The spin version of Rice-Mele model and spin pumping is discussed in Ref.⁸³ shift current by Floquet theory and Keldysh method³⁶

4.3 Dirac systems

The TLZ model can also be utilized for analyzing the Dirac systems with the application of circularly polarized laser field. The geometric tunneling in the Dirac systems is thoroughly studied in Ref.⁷⁰ and we briefly review the results here.

First, let us consider the 2D Dirac fermions in the rotating electric field $\mathbf{E} = E(\cos(\Omega t), \sin(\Omega t))$ ($E > 0$). The vector potential is represented as $\mathbf{A} = A(-\sin(\Omega t), \cos(\Omega t))$, where $A = E/\Omega$ ($\mathbf{E} = -\partial_t \mathbf{A}$). Then the Hamiltonian is written as

$$\hat{H} = v[\xi(k_x + e_0 A_x)\hat{\sigma}^x + (k_y + e_0 A_y)\hat{\sigma}^y] + m\hat{\sigma}^z, \quad (54)$$

where v is the light velocity, which corresponds to the Fermi velocity in condensed matter, and $m > 0$ is the mass. Note that there are two kinds of chirality $\xi = \pm$.

For the fixed wave number (k_x, k_y) , we can regard Eq. (54) as the TLZ model through the expansion up to the second order of Ωt around the gap minimum point $(\cos(\Omega t_0), \sin(\Omega t_0)) = \frac{\Omega}{|k||\Omega|}(-k_y, k_x)$ [See Fig. 4(a)], the Hamiltonian is approximated as

$$\begin{aligned} \hat{H} &= v\xi \left(1 - \frac{e_0 E}{|k||\Omega|}\right) k_x \hat{\sigma}^x + v \left(1 - \frac{e_0 E}{|k||\Omega|}\right) k_y \hat{\sigma}^y + m\hat{\sigma}^z \\ &- v \frac{e_0 E}{|k||\Omega|} (\xi k_y \hat{\sigma}^x - k_x \hat{\sigma}^y) (-\Omega t') \\ &+ v \frac{e_0 E}{|k||\Omega|} (\xi k_x \hat{\sigma}^x + k_y \hat{\sigma}^y) \frac{(\Omega t')^2}{2}, \end{aligned} \quad (55)$$

where $t' = t - t_0$. Note that the angular frequency Ω works as a sweep velocity F in the present case. The sign of Ω corresponds to the helicity of light. Utilizing Eq. (38), we can calculate the tunneling probability as

$$\mathcal{P}_\xi(\Omega, \mathbf{k}) = \exp \left[-\pi \frac{\left(M - \frac{\xi\Omega m}{4M}\right)^2}{v e_0 E} \right], \quad (56)$$

where we have defined $M = \sqrt{v^2(|\mathbf{k}| - e_0 E/|\Omega|)^2 + m^2}$. Note that the tunneling probability Eq. (56) depends on both the chirality ξ and the helicity of light $\text{sgn}(\Omega)$.

We can observe the characteristic phenomena caused by the geometric effects: the chiral imbalance and circular dichroism, which are represented as

$$\frac{\mathcal{P}_+(\Omega, \mathbf{k})}{\mathcal{P}_-(\Omega, \mathbf{k})} = \exp \left(\frac{\pi\Omega m}{v e_0 E} \right) \quad (57)$$

and

$$\frac{\mathcal{P}_\xi(|\Omega|, \mathbf{k})}{\mathcal{P}_\xi(-|\Omega|, \mathbf{k})} = \exp \left(\frac{\pi\xi|\Omega|m}{v e_0 E} \right). \quad (58)$$

These results are analogous to the rectification, which has been seen in the saw-tooth chain Eq. (50). Since the ratio Eqs. (57) and (58) does not depend on \mathbf{k} , the same relation holds for the fermion-antifermion pair production rate

$$\Gamma_\xi(\Omega) \equiv \frac{|\Omega|}{(2\pi)^3} \int d\mathbf{k} \mathcal{P}_\xi(\Omega, \mathbf{k}). \quad (59)$$

Another characteristic geometric effect, perfect tunneling, also plays an important role in fermion-antifermion pair production rate and demonstrates the twisted Schwinger effect. From Eq. (56), the condition for perfect tunneling $\mathcal{P}_\xi(\Omega, \mathbf{k}) = 1$ is $M = \frac{\xi\Omega m}{4M}$, and the solution of this equation is given as

$$|\mathbf{k}| = \begin{cases} \text{No solution} & (\xi\Omega < 4m) \\ \frac{e_0 E}{|\Omega|} + \frac{1}{v} \sqrt{m \left(\frac{\xi\Omega}{4} - m \right)} & (\xi\Omega \geq 4m, E < E_{co}) \\ \frac{e_0 E}{|\Omega|} \pm \frac{1}{v} \sqrt{m \left(\frac{\xi\Omega}{4} - m \right)} & (\xi\Omega \geq 4m, E \geq E_{co}), \end{cases} \quad (60)$$

where $E_{co} = \frac{|\Omega|}{e_0 v} \sqrt{m \left(\frac{\xi\Omega}{4} - m \right)}$. The contribution to pair production rate $\Gamma_\xi(\Omega)$ comes mainly from the wave numbers where perfect tunneling happens. In $\xi\Omega < 4m$, the contribution is from the modified gap minimum $|\mathbf{k}| = e_0 E/|\Omega|$.

The pair production rate $\Gamma_\xi(\Omega)$ can be evaluated by the saddle point method.⁷⁰ Here we only describe the results. For $\xi\Omega \geq 4m$, $\Gamma_\xi(\Omega)$ behaves in a power law of E . As E is increased, the power shows a crossover from $\Gamma_\xi(\Omega) \propto E^{1/2}$ to

$\Gamma_\xi(\Omega) \propto E^{3/2}$ at E_{c0} . For $\xi\Omega < 4m$, the pair production rate is written as

$$\Gamma_\xi \propto E^{3/2} \exp\left(-\pi \frac{E_{th}(\Omega)}{E}\right), \quad (61)$$

where the threshold of electric field is provided as

$$E_{th}(\Omega) = \frac{(m - \xi\Omega/4)^2}{ve_0}. \quad (62)$$

For small E , the pair production is exponentially suppressed. When E is increased, the number fermion-antifermion pairs grow rapidly above $E_{th}(\Omega)$, and it shows a power law behavior $\Gamma_\xi \propto E^{3/2}$. In the limit of $\Omega \rightarrow 0$, the threshold becomes $E_{th}(\Omega) \rightarrow m^2/(ve_0)$ and the results by Schwinger Eqs. (4) and (5) are reproduced. Hence, Eqs. (61) and (62) are an extension of Schwinger's results to the case of rotating electric field. The behavior of the total pair production rate Γ_ξ in the parameter space of $\xi\Omega$ and E is summarized in Fig. 4(b). A resemblance is pointed out between Fig. 4(b) and the phase diagram of a holographic model.^{84,85)}

In several kinds of 2D materials such as monolayer transition metal dichalcogenides and graphene,^{86–88)} the 2D massive Dirac model works as an effective model for the dispersion around K and K' points, which are called valleys. These different valleys correspond to different chirality in the Dirac model. In the above discussion, it is assumed that the Fermi energy is located at zero.

The twisted Schwinger effect also appears in 3D massless Dirac fermions in circularly polarized laser, which is represented by the Hamiltonian

$$\hat{\mathcal{H}}_{3D} = v \sum_{j=x,y,z} \hat{\gamma}^0 \hat{\gamma}^j (k_j + e_0 A_j), \quad (63)$$

$A = A(-\sin(\Omega t), \cos(\Omega t), 0)$. This Hamiltonian is the same as Eq. (3), and we set $m = 0$ and substitute k_j by $k_j + e_0 A_j$. The Hilbert space of the 3D massless Dirac model Eq. (63) is divided into two chiral sectors as

$$\hat{\mathcal{H}}_{3D} = \begin{pmatrix} \hat{\mathcal{H}}_- & 0 \\ 0 & \hat{\mathcal{H}}_+ \end{pmatrix}, \quad (64)$$

where $\hat{\mathcal{H}}_\pm = \pm v \sum_{j=x,y,z} (k_j + e_0 A_j) \hat{\sigma}^j$. Through the rotation of $\hat{\mathcal{H}}_-$ about the $\hat{\sigma}^z$ axis by the angle π , the Hamiltonian transforms into

$$\hat{U}^\dagger \hat{\mathcal{H}}_{3D} \hat{U} = \begin{pmatrix} \hat{\mathcal{H}}'_- & 0 \\ 0 & \hat{\mathcal{H}}'_+ \end{pmatrix}, \quad \hat{U} = \begin{pmatrix} e^{i\frac{\pi}{2}\hat{\sigma}^z} & 0 \\ 0 & I \end{pmatrix}. \quad (65)$$

The Hamiltonian in each sector $\hat{\mathcal{H}}'_+$ and $\hat{\mathcal{H}}'_-$ is the same as the massive 2D Dirac model Eq. (54) with the replacement $m \rightarrow k_z$. Thus we can analyze the massless 3D Dirac model in the same way as the 2D case. We remark that the summation over k_z and $\xi = \pm$ should be taken in order to evaluate the physical quantities. For example, the pair production rate and the current along the z axis in each chiral sector are defined as

$$\Gamma_\xi(\Omega) = \frac{|\Omega|^4}{(2\pi)^4 v^3} \int dk \tilde{\mathcal{P}}_\xi(\Omega, k) \quad (66)$$

$$J_\xi^z(\Omega) = -\frac{2e\tau|\Omega|^4}{(2\pi)^4 v^2} \int dk \frac{k_z}{|\mathbf{k}|} \tilde{\mathcal{P}}_\xi(\Omega, k), \quad (67)$$

where τ is the lifetime of the generated pairs and $\tilde{\mathcal{P}}_\xi(\Omega, k)$ is obtained by replacing m in Eq. (56) by k_z . Since there

is a symmetry $\tilde{\mathcal{P}}_{-\xi}(\Omega, k_x, k_y, k_z) = \tilde{\mathcal{P}}_\xi(\Omega, k_x, k_y, -k_z)$ from Eq. (56), the chiral pair production rate $\Gamma_+(\Omega) - \Gamma_-(\Omega)$ and the total current $J_+^z(\Omega) + J_-^z(\Omega)$ becomes zero. Hence we focus on the total pair production rate $\Gamma_+(\Omega) + \Gamma_-(\Omega)$ and the chiral current $J_+^z(\Omega) - J_-^z(\Omega)$. Similarly to the case of 2D Dirac models, the contributions from the perfect tunneling points dominates. Since the integration over all the wave numbers k_x, k_y, k_z is taken, the perfect tunneling points always exist in the integral region. Thus the total pair production rate and the chiral current behaves in the power law of the applied electric field E . In addition, the crossover of power is observed when E is increased in the same way as the 2D case.⁷⁰⁾

The results explained above has an implication for the systems excited by a circularly polarized laser^{89–91)} and optical lattices with potential shaking.⁹²⁾ The chiral imbalance of pair production is related to the valley polarization.^{93,94)} There are a lot of studies on other nonperturbative phenomena caused by circularly polarized laser fields.^{38–40,95–98)}

5. Keldysh crossover in many-body systems

In the preceding discussion, we focused on quantum tunneling phenomena induced by the application of an external field. Another important approach for analyzing the dynamics is the Floquet theory, which is useful for describing multiphoton absorption processes in the high-frequency regime. A crossover occurs when the parameters cross the Keldysh line, which separates the tunneling regime from the Floquet regime (Fig. 1). This crossover, which is first studied by Keldysh in the ionization process of atoms,²⁷⁾ is therefore referred to as the Keldysh crossover. Following the seminal work by Keldysh, studies have been conducted on such crossover behavior in pair production under an AC electric field.^{20,21,99)} The Keldysh crossover is also studied in condensed matter systems such as Mott insulators under a laser field,¹³⁾ and there are experimental observations in Mott insulators¹⁰⁰⁾ and Weyl semimetals¹⁰¹⁾ with an application of AC electric field.

Here we consider the spin-1 Heisenberg antiferromagnetic chain, which has an excitation gap in contrast to the case of half-odd spin chains from Haldane's theory.^{102,103)} The ground state of the spin-1 chain has a topological order protected by the symmetry of the system.^{104–106)} We apply a magnetic field gradient to the spin-1 Heisenberg antiferromagnetic chain, and then Hamiltonian is represented as

$$\hat{\mathcal{H}} = J \sum_j \left[\frac{1}{2} (\hat{S}_j^+ \hat{S}_{j+1}^- + \hat{S}_j^- \hat{S}_{j+1}^+) + \hat{S}_j^z \hat{S}_{j+1}^z \right] - F \sum_j j \hat{S}_j^z. \quad (68)$$

Since $\sum_j \hat{S}_j^z$ is a conserved quantity for this Hamiltonian, \hat{S}_j^z can be regarded as a charge at the site j . The $\hat{S}_j^+ \hat{S}_{j+1}^-$ and $\hat{S}_j^- \hat{S}_{j+1}^+$ terms correspond to the hopping of the charge, and the $\hat{S}_j^z \hat{S}_{j+1}^z$ term corresponds to the nearest neighbor interaction. Since the $\sum_j j \hat{S}_j^z$ works as a polarization, we call F the spin-electric field. In the velocity gauge, the Hamiltonian is represented as

$$\hat{\mathcal{H}}(t) = J \sum_j \left[\frac{1}{2} (e^{iFt} \hat{S}_j^+ \hat{S}_{j+1}^- + e^{-iFt} \hat{S}_j^- \hat{S}_{j+1}^+) + \hat{S}_j^z \hat{S}_{j+1}^z \right]. \quad (69)$$

We consider the time evolution starting from the ground state

$\hat{H}(0)$ in the time interval of $0 \leq t \leq 2\pi/(LF)$, where L is the system size. This process is the insertion of a single flux $\phi = 2\pi/L$.¹⁰⁷⁾

Let us consider this situation from the perspective of a tunneling problem. The instantaneous energy level structure of $\hat{H}(2\pi/(LF))$ is the same as that of $\hat{H}(0)$, and the excitation gap takes minimum at $t = \pi/(LF)$. Hence the time evolution in $0 \leq t \leq 2\pi/(LF)$ can be regarded as tunneling phenomena, and the transition probability from the lower to upper band can be evaluated by the DDP method as

$$P(F) = \exp(-\pi F_{\text{th}}/F), \quad (70)$$

where F_{th} is the threshold.

This time evolution can also be analyzed in terms of the Floquet theory. Since the Hamiltonian has a periodicity $\hat{H}(0) = \hat{H}(2\pi/F)$, F works as an angular frequency and we can define the Floquet effective Hamiltonian \hat{H}_F by

$$\mathcal{T} \exp\left(-i \int_{t_0}^{t_0+2\pi/F} \hat{H}(s) ds\right) = \exp(-i\hat{H}_F t), \quad (71)$$

where \mathcal{T} is the time-ordering. We can calculate \hat{H}_F using the inverse frequency expansion^{37, 108, 109)} and evaluate the transition probability from the lower to upper band as

$$P(F) = c_0 \exp(-\pi F_q/F), \quad (72)$$

where c_0 and F_q are constant real numbers ($0 \leq c_0 \leq 1$).¹⁰⁷⁾

Comparing the numerically calculated $P(F)$ with the expressions Eqs. (70) and (72), it is found that $P(F)$ is well described by Eq. (70) (Eq. (72)) in the region of $F < F_*$ ($F > F_*$), where F_* is the crossing point of the two curves represented by Eqs. (70) and (72).¹⁰⁷⁾ As F is increased, the crossover from the tunneling regime to the Floquet regime happens at F_* . This crossover corresponds to the parameter change along the horizontal line in Fig. 1 since F serves as the angular frequency in the present case. Therefore this phenomenon is the Keldysh crossover in the quantum spin systems provoked by a DC spin electric field.

6. Summary and discussion

We have discussed geometric effects of quantum tunneling, especially on the tunneling amplitude. After the review of the LZ model and Schwinger effect, the modern perspective on polarization, and the adiabatic perturbation theory, we have introduced the TLZ model and showed that the shift vector appears in the expression of tunneling probability. We have demonstrated several applications of the TLZ model, where nonreciprocity and perfect tunneling play an essential role. Lastly, we explain the Keldysh crossover seen in condensed matter systems.

The tunneling phenomenon is closely related to the manipulation of quantum states. Hence developing the way to control quantum states rapidly and coherently by utilizing geometric effects in tunneling is an important challenge. In particular, geometric tunneling in strongly correlated systems still remains unexplored and should be further investigated in the future research. Furthermore, studying the interplay between geometric effects in quantum dynamics and the intrinsic topology of the system is also an intriguing future problem.

This work was supported by a Grant-in-Aid for Scientific

Research from JSPS, KAKENHI Grant Nos. JP23H04865, JP23K22418, JP23K22487, JP24H00191, JP24K06891, and JST CREST Grant No. JPMJCR19T3, Japan.

- 1) L. D. Landau, Phys. Z. Sowjet. **2**, 46 (1932).
- 2) N. Rosen and C. Zener, Phys. Rev. **40**, 502 (1932).
- 3) E. C. G. Stückelberg, Helv. Phys. Acta **5**, 369 (1932).
- 4) C. Zener, Proc. Roy. Soc. Lond. A **145**, 523 (1934).
- 5) G.-X. Miao, M. Münzenberg, and J. S. Moodera, Rep. Prog. Phys. **74**, 036501 (2011).
- 6) F. Gaitan, Phys. Rev. A **68**, 052314 (2003).
- 7) R. Li and F. Gaitan, J. Mod. Opt. **58**, 1922 (2011).
- 8) W. Heisenberg and H. Euler, Z. Phys. **98**, 714 (1936).
- 9) J. Schwinger, Phys. Rev. **82**, 664 (1951).
- 10) E. Kane, J. Phys. Chem. Sol. **12**, 181 (1960).
- 11) T. Oka, R. Arita, and H. Aoki, Phys. Rev. Lett. **91**, 066406 (2003).
- 12) T. Oka and H. Aoki, Phys. Rev. Lett. **95**, 137601 (2005).
- 13) T. Oka, Phys. Rev. B **86**, 075148 (2012).
- 14) B. Mayer, C. Schmidt, A. Grupp, J. Bühler, J. Oelmann, R. E. Marvel, R. F. Haglund, T. Oka, D. Brida, A. Leitenstorfer, and A. Pashkin, Phys. Rev. B **91**, 235113 (2015).
- 15) H. Yamakawa, T. Miyamoto, T. Morimoto, T. Terashige, H. Yada, N. Kida, M. Suda, H. Yamamoto, R. Kato, K. Miyagawa, K. Kanoda, and H. Okamoto, Nat. Mater. **16**, 1100 (2017).
- 16) N. Takamura, T. Miyamoto, S. Liang, K. Asada, T. Terashige, Y. Takahashi, T. Hasegawa, and H. Okamoto, Phys. Rev. B **107**, 085147 (2023).
- 17) T. W. B. Kibble, J. Phys. A: Math. Gen. **9**, 1387 (1976).
- 18) W. H. Zurek, Nature (London) **317**, 505 (1985).
- 19) B. Damski, Phys. Rev. Lett. **95**, 035701 (2005).
- 20) E. Brezin and C. Itzykson, Phys. Rev. D **2**, 1191 (1970).
- 21) V. S. Popov, Sov. J. Nucl. Phys. **19**, 584 (1974).
- 22) R. Schützhold, H. Gies, and G. Dunne, Phys. Rev. Lett. **101**, 130404 (2008).
- 23) M. S. Misha Yu Ivanov and O. Smirnova, J. Mod. Opt. **52**, 165 (2005).
- 24) F. Krausz and M. Ivanov, Rev. Mod. Phys. **81**, 163 (2009).
- 25) C. I. Blaga, F. Catoire, P. Colosimo, G. G. Paulus, H. G. Muller, P. Agostini, and L. F. DiMauro, Nat. Phys. **5**, 335 (2009).
- 26) S. V. Popruzhenko, J. Phys. B: Atom. Molec. Opt. Phys. **47**, 204001 (2014).
- 27) L. Keldysh, Sov. Phys. JETP **20**, 1307 (1965).
- 28) M. V. Berry, Proc. R. Soc. Lond. A **392**, 45 (1984).
- 29) D. Xiao, M.-C. Chang, and Q. Niu, Rev. Mod. Phys. **82**, 1959 (2010).
- 30) D. J. Thouless, M. Kohmoto, M. P. Nightingale, and M. den Nijs, Phys. Rev. Lett. **49**, 405 (1982).
- 31) M. Kohmoto, Ann. Phys. **160**, 343 (1985).
- 32) M. Z. Hasan and C. L. Kane, Rev. Mod. Phys. **82**, 3045 (2010).
- 33) X.-L. Qi and S.-C. Zhang, Rev. Mod. Phys. **83**, 1057 (2011).
- 34) I. Sodemann and L. Fu, Phys. Rev. Lett. **115**, 216806 (2015).
- 35) J. E. Sipe and A. I. Shkrebtii, Phys. Rev. B **61**, 5337 (2000).
- 36) T. Morimoto and N. Nagaosa, Sci. Adv. **2**, e1501524 (2016).
- 37) T. Oka and S. Kitamura, Ann. Rev. Condens. Matter Phys. **10**, 387 (2019).
- 38) T. Oka and H. Aoki, Phys. Rev. B **79**, 081406 (2009).
- 39) T. Kitagawa, T. Oka, A. Brataas, L. Fu, and E. Demler, Phys. Rev. B **84**, 235108 (2011).
- 40) N. H. Lindner, G. Refael, and V. Galitski, Nat. Phys. **7**, 490 (2011).
- 41) Y. Aharonov and J. Anandan, Phys. Rev. Lett. **58**, 1593 (1987).
- 42) M. V. Berry, Proc. Roy. Soc. Lond. A **430**, 405 (1990).
- 43) K. Nakamura and S. A. Rice, Phys. Rev. A **49**, R2217 (1994).
- 44) D. Bouwmeester, G. P. Karman, N. H. Dekker, C. A. Schrama, and J. P. Woerdman, J. Mod. Opt. **43**, 2087 (1996).
- 45) M. Demirplak and S. A. Rice, J. Phys. Chem. A **107**, 9937 (2003).
- 46) M. V. Berry, J. Phys. A: Math. and Theor. **42**, 365303 (2009).
- 47) A. del Campo, Phys. Rev. Lett. **111**, 100502 (2013).
- 48) F. Sauter, Z. Phys. **69**, 742 (1931).
- 49) R. D. King-Smith and D. Vanderbilt, Phys. Rev. B **47**, 1651 (1993).
- 50) D. Vanderbilt and R. D. King-Smith, Phys. Rev. B **48**, 4442 (1993).
- 51) R. Resta, Phys. Rev. Lett. **80**, 1800 (1998).
- 52) R. Resta and S. Sorella, Phys. Rev. Lett. **82**, 370 (1999).

- 53) E. Lieb, T. Schultz, and D. Mattis, *Ann. Phys. (N. Y.)* **16**, 407 (1961).
- 54) M. Oshikawa, M. Yamanaka, and I. Affleck, *Phys. Rev. Lett.* **78**, 1984 (1997).
- 55) M. Oshikawa, *Phys. Rev. Lett.* **84**, 1535 (2000).
- 56) M. B. Hastings, *Europhys. Lett.* **70**, 824 (2005).
- 57) M. Nakamura and J. Voit, *Phys. Rev. B* **65**, 153110 (2002).
- 58) M. Nakamura and S. Todo, *Phys. Rev. Lett.* **89**, 077204 (2002).
- 59) T. Oka and H. Aoki, *Phys. Rev. B* **81**, 033103 (2010).
- 60) A. M. Dykhne, *Sov. Phys. JETP* **14**, 941 (1962).
- 61) J. P. Davis and P. Pechukas, *J. Chem. Phys.* **64**, 3129 (1976).
- 62) A. Joye, H. Kunz, and C.-E. Pfister, *Ann. Phys. (N. Y.)* **208**, 299 (1991).
- 63) K. Fukushima and T. Shimazaki, *Ann. Phys.* **415**, 168111 (2020).
- 64) S. Kitamura, N. Nagaosa, and T. Morimoto, *Commun. Phys.* **3**, 1 (2020).
- 65) J.-d. Wu, M.-s. Zhao, J.-l. Chen, and Y.-d. Zhang, *Phys. Rev. A* **77**, 062114 (2008).
- 66) C. Xu, J. Wu, and C. Wu, *Phys. Rev. A* **97**, 032124 (2018).
- 67) I. Terada, S. Kitamura, H. Watanabe, and H. Ikeda, *Phys. Rev. B* **111**, 064315 (2025).
- 68) S. Takayoshi, H. Aoki, and T. Oka, *Phys. Rev. B* **90**, 085150 (2014).
- 69) S. Takayoshi, M. Sato, and T. Oka, *Phys. Rev. B* **90**, 214413 (2014).
- 70) S. Takayoshi, J. Wu, and T. Oka, *SciPost Phys.* **11**, 075 (2021).
- 71) E. Torrontegui, S. Ibanez, S. Martínez-Garaot, M. Modugno, A. del Campo, D. Guéry-Odelin, A. Ruschhaupt, X. Chen, and J. G. Muga, *Adv. At. Mol. Opt. Phys.* **62**, 117 (2013).
- 72) D. Guéry-Odelin, A. Ruschhaupt, A. Kiely, E. Torrontegui, S. Martínez-Garaot, and J. G. Muga, *Rev. Mod. Phys.* **91**, 045001 (2019).
- 73) S. Miyashita, *J. Phys. Soc. Jpn.* **64**, 3207 (1995).
- 74) H. De Raedt, S. Miyashita, K. Saito, D. García-Pablos, and N. García, *Phys. Rev. B* **56**, 11761 (1997).
- 75) K. Sasaki, Y. Nakamura, T. Teraji, T. Oka, and K. Kobayashi, *Phys. Rev. A* **107**, 053113 (2023).
- 76) I. Terada, S. Kitamura, H. Watanabe, and H. Ikeda, *Phys. Rev. B* **109**, L180302 (2024).
- 77) I. Terada, S. Kitamura, H. Watanabe, and H. Ikeda, *phys. status solidi (b)* **262**, 2400533 (2025).
- 78) M. J. Rice and E. J. Mele, *Phys. Rev. Lett.* **49**, 1455 (1982).
- 79) S. Nakajima, T. Tomita, S. Taie, T. Ichinose, H. Ozawa, L. Wang, M. Troyer, and Y. Takahashi, *Nat. Phys.* **12**, 296 (2016).
- 80) L. Wang, M. Troyer, and X. Dai, *Phys. Rev. Lett.* **111**, 026802 (2013).
- 81) T. Morimoto and N. Nagaosa, *Phys. Rev. B* **100**, 235138 (2019).
- 82) H. Ishizuka and M. Sato, *Phys. Rev. Lett.* **122**, 197702 (2019).
- 83) R. Shindou, *J. Phys. Soc. Jpn.* **74**, 1214 (2005).
- 84) K. Hashimoto, S. Kinoshita, K. Murata, and T. Oka, *JHEP* **2017**, 127 (2017).
- 85) S. Kinoshita, K. Murata, and T. Oka, *JHEP* **2018**, 96 (2018).
- 86) A. Rycerz, J. Tworzydło, and C. Beenakker, *Nat. Phys.* **3**, 172 (2007).
- 87) J. R. Schaibley, H. Yu, G. Clark, P. Rivera, J. S. Ross, K. L. Seyler, W. Yao, and X. Xu, *Nat. Rev. Mater.* **1**, 16055 (2016).
- 88) Y. Liu, Y. Gao, S. Zhang, J. He, J. Yu, and Z. Liu, *Nano Res.* **12**, 2695 (2019).
- 89) J. Karch, P. Olbrich, M. Schmalzbauer, C. Zoth, C. Brinsteiner, M. Fehrenbacher, U. Wurstbauer, M. M. Glazov, S. A. Tarasenko, E. L. Ivchenko, D. Weiss, J. Eroms, R. Yakimova, S. Lara-Avila, S. Kubatkin, and S. D. Ganichev, *Phys. Rev. Lett.* **105**, 227402 (2010).
- 90) Y. H. Wang, H. Steinberg, P. Jarillo-Herrero, and N. Gedik, *Science* **342**, 453 (2013).
- 91) J. W. McIver, B. Schulte, F.-U. Stein, T. Matsuyama, G. Jotzu, G. Meier, and A. Cavalleri, *Nat. Phys.* **16**, 38 (2020).
- 92) G. Jotzu, M. Messer, R. Desbuquois, M. Lebrat, T. Uehlinger, D. Greif, and T. Esslinger, *Nature* **515**, 237 (2014).
- 93) W. Yao, D. Xiao, and Q. Niu, *Phys. Rev. B* **77**, 235406 (2008).
- 94) D. Xiao, G.-B. Liu, W. Feng, X. Xu, and W. Yao, *Phys. Rev. Lett.* **108**, 196802 (2012).
- 95) R. Wang, B. Wang, R. Shen, L. Sheng, and D. Y. Xing, *Europhys. Lett.* **105**, 17004 (2014).
- 96) S. Ebihara, K. Fukushima, and T. Oka, *Phys. Rev. B* **93**, 155107 (2016).
- 97) C.-K. Chan, P. A. Lee, K. S. Burch, J. H. Han, and Y. Ran, *Phys. Rev. Lett.* **116**, 026805 (2016).
- 98) L. Bucciattini, S. Roy, S. Kitamura, and T. Oka, *Phys. Rev. B* **96**, 041126 (2017).
- 99) V. S. Popov, *Phys. Usp.* **47**, 855 (2004).
- 100) X. Li, H. Ning, O. Mehio, H. Zhao, M.-C. Lee, K. Kim, F. Nakamura, Y. Maeno, G. Cao, and D. Hsieh, *Phys. Rev. Lett.* **128**, 187402 (2022).
- 101) R. Ikeda, H. Watanabe, M. J. Heon, M.-H. Jung, K. Takasan, and S.-i. Kimura, *J. Phys. Soc. Jpn.* **93**, 053701 (2024).
- 102) F. Haldane, *Phys. Lett. A* **93**, 464 (1983).
- 103) F. D. M. Haldane, *Phys. Rev. Lett.* **50**, 1153 (1983).
- 104) Z.-C. Gu and X.-G. Wen, *Phys. Rev. B* **80**, 155131 (2009).
- 105) F. Pollmann, A. M. Turner, E. Berg, and M. Oshikawa, *Phys. Rev. B* **81**, 064439 (2010).
- 106) F. Pollmann, E. Berg, A. M. Turner, and M. Oshikawa, *Phys. Rev. B* **85**, 075125 (2012).
- 107) K. Okazaki, S. Okumura, S. Takayoshi, and T. Oka, *Phys. Rev. B* **111**, 235422 (2025).
- 108) M. Bukov, L. D'Alessio, and A. Polkovnikov, *Adv. Phys.* **64**, 139 (2015).
- 109) T. Mikami, S. Kitamura, K. Yasuda, N. Tsuji, T. Oka, and H. Aoki, *Phys. Rev. B* **93**, 144307 (2016).